The FEBS Journal

FEBS PRESS science publishing by scientists

Insights into the GTP-dependent allosteric control of c-di-GMP hydrolysis from the crystal structure of PA0575 protein from *Pseudomonas aeruginosa*

Federico Mantoni[1,2], Alessandro Paiardini[1,2], Paolo Brunotti[1], Cecilia D'Angelo[1], Laura Cervoni[1], Alessio Paone[1], Loredana Cappellacci[3], Riccardo Petrelli[3], Massimo Ricciutelli[3], Livia Leoni[4], Giordano Rampioni[4], Alessandro Arcovito[5], Serena Rinaldo[1,2], Francesca Cutruzzolà[1,2] and Giorgio Giardina[1,2]

1 Department of Biochemical Sciences "A. Rossi Fanelli", Sapienza University of Rome, Italy
2 Istituto Pasteur Italia-Fondazione Cenci Bolognetti, Rome, Italy
3 School of Pharmacy, Medicinal Chemistry Unit, University of Camerino, Italy
4 Department of Science, University Roma Tre, Italy
5 Istituto di Biochimica e Biochimica Clinica, Università Cattolica del Sacro Cuore, Rome, Italy

Keywords
c-di-GMP; GTP; hybrid protein; phosphodiesterase; RmcA

Correspondence
S. Rinaldo and F. Cutruzzolà, Department of Biochemical Sciences "A. Rossi Fanelli", Sapienza University of Rome, P.le Aldo Moro 5, 00185, Rome, Italy
Fax: +39 064440062 (SR and FC)
Tel: +39 0649910713 (SR) and +39 0649910955 (FC)
Emails: serena.rinaldo@uniroma1.it (SR) and francesca.cutruzzola@uniroma1.it (FC)

Federico Mantoni, Alessandro Paiardini and Paolo Brunotti contributed equally to this work

(Received 4 June 2018, revised 25 July 2018, accepted 10 August 2018)

doi:10.1111/febs.14634

Bis-(3′-5′)-cyclic diguanylic acid (c-di-GMP) belongs to the class of cyclic dinucleotides, key carriers of cellular information in prokaryotic and eukaryotic signal transduction pathways. In bacteria, the intracellular levels of c-di-GMP and their complex physiological outputs are dynamically regulated by environmental and internal stimuli, which control the antagonistic activities of diguanylate cyclases (DGCs) and c-di-GMP specific phosphodiesterases (PDEs). Allostery is one of the major modulators of the c-di-GMP-dependent response. Both the c-di-GMP molecule and the proteins interacting with this second messenger are characterized by an extraordinary structural plasticity, which has to be taken into account when defining and possibly predicting c-di-GMP-related processes. Here, we report a structure-function relationship study on the catalytic portion of the PA0575 protein from *Pseudomonas aeruginosa*, bearing both putative DGC and PDE domains. The kinetic and structural studies indicate that the GGDEF-EAL portion is a GTP-dependent PDE. Moreover, the crystal structure confirms the high degree of conformational flexibility of this module. We combined structural analysis and protein engineering studies to propose the possible molecular mechanism guiding the nucleotide-dependent allosteric control of catalysis; we propose that the role exerted by GTP via the GGDEF domain is to allow the two EAL domains to form a dimer, the species competent to enter PDE catalysis.

Introduction

The bis-(3′-5′)-cyclic diguanylic acid (c-di-GMP) is a ubiquitous bacterial dinucleotide, controlling complex processes such as the transition from single-cell motile state to biofilm and cellular differentiation [1]. The intracellular levels of c-di-GMP are controlled by the opposite activities of diguanylate cyclases (DGCs), containing GGDEF domains, and phosphodiesterases (PDEs), containing either EAL or HD-GYP domains [1]. The activity of DGCs and PDEs is often allosterically regulated in a remarkably

Abbreviations
c-di-GMP, bis-(3′-5′)-cyclic diguanylic acid; DGC, diguanylate cyclase; PDE, phosphodiesterase; pGpG, 5′-phosphoguanylyl-(3′-5′)-guanosine; RmcA, Redox regulator of c-di-GMP.

complex way by environmental/metabolic signals acting on the large variety of sensory domains neighbouring the catalytic ones [1,2]. Representative of this complexity are the so-called hybrid proteins, where the GGDEF and EAL domains are fused into the same polypeptide chain. The GGDEF-EAL hybrid proteins, which contain about 1/3 of all GGDEF and 2/3 of all EAL domains, are the least characterized members of the c-di-GMP signalling network [3]. In these proteins, the GGDEF-EAL pair may display a wide range of functional behaviours: the two domains may act as a genuine DGC and PDE, as in *Pseudomonas aeruginosa* MorA [4], or the GGDEF domain may regulate the PDE activity of the EAL domain, as in CC3396 from *Caulobacter crescentus* and in *P. aeruginosa* RbdA [5–7]. Lastly, the GGDEF-EAL pair could behave as a specific c-di-GMP receptor with no enzymatic activity, as in *P. aeruginosa* FimX [8] and *Pseudomonas fluorescens* LapD [9].

The structures of hybrid proteins solved so far underline the importance of the interdomain interactions between GGDEF and EAL modules in controlling the observed large conformational changes induced upon ligand binding. Fusion of the GGDEF and EAL domains often allows fine-tuning of the enzyme, in order to link the catalytic activity of these polypeptides to the availability of the different nucleotides (mainly GTP and c-di-GMP). Understanding the structure and reciprocal regulation of the GGDEF-EAL domains is needed to clarify their biochemical properties and their role in the c-di-GMP-mediated signal transduction, up to now poorly investigated from a mechanistic point of view.

Here, we present a detailed structural and functional study on the GGDEF-EAL tandem domains of *P. aeruginosa* PAO1 PA0575 protein, a multidomain hybrid protein containing a periplasmic sensory domain, a transmembrane helix, four Per-Arnt-Sim (PAS) domains, the last of which represents the light/oxygen or voltage sensing (LOV) version of PAS, and finally the GGDEF-EAL effector superdomain (Fig. 1A). We recently found that this protein is able to control (by lowering) c-di-GMP levels in response to L-Arginine as carbon source [10]. The corresponding genetic mutant in *P. aeruginosa* PA14 (mutated in PA14_07500 gene, sharing 99% of sequence identity with PA0575) shows severely reduced swarming and swimming motility [11]; more recently, the same PA14_07500 gene has been shown to control matrix production and colony morphogenesis in response to the cellular redox state and phenazines, and accordingly named RmcA (Redox regulator of c-di-GMP) [12]. Given the high percentage of sequence identity of PA0575 with the PA14 counterpart, hereinafter we will adopt the RmcA name also for PA0575.

The characterization of the catalytic moiety of *P. aeruginosa* RmcA reported here confirms that the activity of this protein is to degrade c-di-GMP and that the PDE activity is allosterically controlled by GTP through the GGDEF domain. The structural and protein engineering analysis reported here were used to profile the structural and functional basis for the allosteric control of the PDE catalytic activity by the GGDEF domain.

Results

The PDE activity of the EAL domain is allosterically controlled by GTP

To characterize the activity of RmcA GGDEF and EAL domains, different constructs were produced (Fig. 1A), containing both domains (DUAL) or the sole EAL domain with or without the upstream hinge helix (EAL-1 and EAL-2, respectively). Conservation of the signature sequences on both domains suggested that the DUAL construct could display both the DGC and the PDE catalytic activities. In agreement with our preliminary evidence on *P. aeruginosa* PAO1-ΔPA0575 mutant showing c-di-GMP accumulation in the presence of L-Arginine as carbon source [10], we found that: (a) the DUAL protein is able to hydrolyse c-di-GMP into pGpG *in vitro* (Fig. 1B); (b) as expected, the PDE activity is a property of the EAL domain, as it is conserved in the EAL-1 and EAL-2 constructs (Fig. 1B); (c) under the same experimental conditions, no DGC or PDE-B activity (i.e. hydrolytic conversion of pGpG into GMP [13]) is observed when GTP is the sole substrate (Fig. 1B–D).

The PDE activity of DUAL increases in the presence of excess GTP (Fig. 2A,B, Table 1 and Table S1); this positive effect is also seen if GTP is added during c-di-GMP hydrolysis, suggesting that feedback inhibition by c-di-GMP does not occur (Fig. 2C). GDP, ppGpp and pppGpp are also able to trigger EAL activation to some extent (Fig. 2D). The allosteric effect of GTP on the PDE activity of DUAL involves the GGDEF domain (Fig. 3A), where it binds with a 1 : 1 stoichiometry (one molecule/monomer) and sub-μM affinity, as assessed by FRET spectroscopy using MANT-GTP (a fluorescent GTP analogue, Fig. 3B); the presence of excess c-di-GMP has no

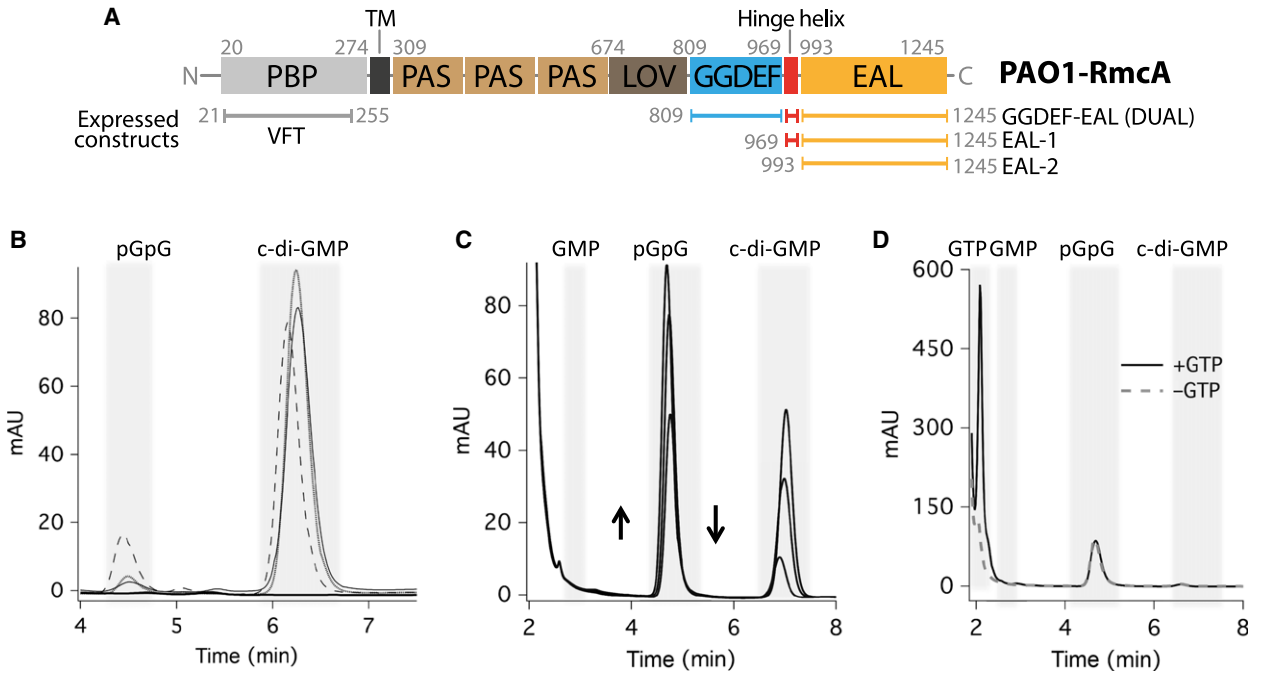

Fig. 1. RmcA GGDEF-EAL construct is a PDE. (A) RmcA domain organization (at the top of the panel) and the constructs characterized so far (in this study and in [10]): DUAL, EAL-1 and EAL-2 (at the bottom of the panel). (B) Pilot enzymatic assays of the RmcA constructs; the nucleotide content of the reaction mixture, containing DUAL incubated with excess of GTP (80 μM; bold line), or with excess of c-di-GMP (30 μM, thin line), to assess the DGC or the PDE activity, respectively, was separated on C8 RP-HPLC. While the PDE reaction yields the expected product (i.e. pGpG), no c-di-GMP production was detected starting from GTP, under these experimental conditions. The PDE activity was also detected on EAL-2, dashed line, and EAL-1, dotted line, incubated with excess c-di-GMP. The reaction was carried out for 30 min in the presence of 1 μM protein, 10 mM $MgCl_2$, 2.5 mM $MnCl_2$, 20 mM Tris pH 7.5, 100 mM NaCl at 25 °C. (C) Nucleotide content of the reaction of DUAL (10 μM) with 30 μM c-di-GMP at different time (30′, 60′, 120′), under the conditions reported in (A); direction of arrows reports the effect on c-di-GMP (consumption) and pGpG (accumulation) during the reaction. No GMP accumulates. (D) Nucleotide content at 60′ of the reaction of EAL-2 (10 μM) with 30 μM c-di-GMP with or without 100 μM GTP (continuous or dashed line, respectively). No GMP accumulates.

effect on MANT-GTP binding (Fig. 3B). As expected, GTP is able to displace MANT-GTP confirming the sub-μM affinity also for the physiological ligand (Fig. 3C).

We found that the PDE activity depends hyperbolically on GTP concentration in the range assayed (2–50 μM, Fig. 3D) yielding an apparent K_{D_app} of 2.8 ± 0.5 μM. Despite the observed sub-μM binding affinity, the maximal GTP-dependent activation of the PDE activity is obtained at GTP concentrations above ~ 15 μM (Fig. 3D). These results suggest that the GTP-dependent PDE activation (measured by the aforementioned K_{D_app}) includes other events than the sole GTP binding, most likely a conformational transition between an inactive to an active form (OFF→ON). Accordingly, the K_M for c-di-GMP is not affected by GTP, while the V_{max} of the PDE reaction increases (Table 1), suggesting that GTP likely increases the population of the catalytically competent PDE enzyme (i.e., the ON form).

C-di-GMP binding to the sole EAL domain (EAL-2) shows one binding site per monomer with a $K_{D\_c\text{-}di\text{-}GMP}$ = 171 ± 30 nM (Fig. 4, including both ITC and FRET data). On the other hand, the ITC profile of the DUAL/c-di-GMP interaction is significantly different and includes complex multiple events, while FRET titration shows a sub-μM affinity for MANT-c-di-GMP (Fig. 4B) and 0.6 : 1 stoichiometry. Altogether these data indicate that c-di-GMP binding to the EAL active site is affected by the presence of the GGDEF domain; the evidence that mutation of key residues located in the EAL pocket abolishes c-di-GMP binding indicates that also in the DUAL construct this nucleotide targets only the EAL domain (Fig. 4C). Interestingly, preincubation of DUAL with excess GTP changes the stoichiometry of binding to 1 : 1, indicating that the GTP-dependent conformational change yields a homogeneous population of EAL active sites able to bind c-di-GMP, while the ITC profile does not change significantly (Fig. 4).

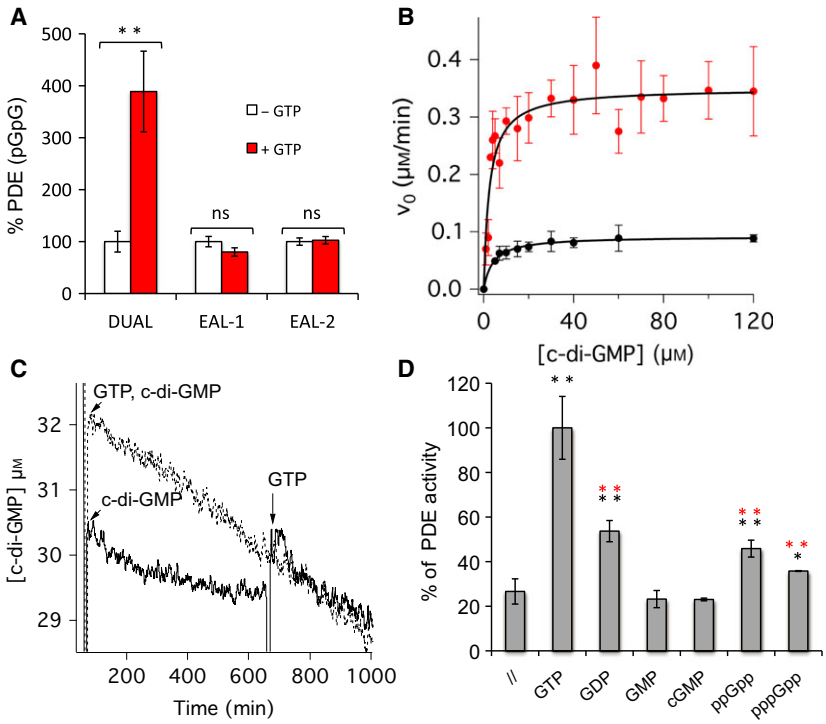

Fig. 2. GTP dependent PDE activity. (A) PDE activity of each construct carried out in the presence of 30 μM c-di-GMP as substrate with or without 50 μM GTP (white and red bars, respectively). Values are normalized to the activity without GTP; data are the means of two experiments ± SD. Statistical significance for each construct with respect to the assay without GTP is indicated (** in the figure, $P < 0.01$); ns: not significant. (B) Determination of the kinetic parameters of DUAL. The PDE activity of DUAL (1 μM) was characterized both in the presence and in the absence of 50 μM GTP (initial rate, v_0, red and black circles, respectively) as a function of c-di-GMP; data were fitted with the Michaelis–Menten equation (continuous line) and the corresponding parameters are reported in Table 1; data are the means of at least three experiments ± SD. (C) The effect of c-di-GMP on GTP activation has been evaluated kinetically. PDE time-course of 1 μM DUAL and 30 μM c-di-GMP: after 10 min from the beginning of the kinetics, 50 μM GTP was added and kinetics followed for further 5 min (continuous trace). The increased rate of c-di-GMP consumption due to GTP addition is comparable to that observed when DUAL is incubated with excess GTP from the beginning of the kinetics (dotted trace). (D) PDE activity was carried out in the presence of different nucleotides (100 μM), as indicated in the *X*-axis. The activity refers to the % of observed PDE activity *vs* that observed in the presence of GTP (100%). Data are the means of two experiments ± SD. Statistical significance with respect to the assay without nucleotides is indicated (black ** and *, for $P < 0.01$ and $P < 0.05$, respectively). For GDP, ppGpp and pppGpp, the statistical significance with respect to the assay with GTP is also included (red, **$P < 0.01$), to demonstrate that GTP is the nucleotide able to populate the maximal PDE activity.

Crystal structure of the GGDEF-EAL domains: clues for the GTP-dependent allosteric changes

We solved the structure of the DUAL construct in complex with two molecules of GTP and five calcium ions at 2.8 Å resolution. DUAL crystallized as an asymmetric dimer, since the relative orientation of the N-terminal GGDEF domain (residue 809–972) with respect to the C-terminal EAL domain (residue 993–1234) in each monomer is very different (Fig. 5A). The overall fold of the GGDEF and EAL domains is conserved in both subunits; superposition of the two EAL domains highlights that the large conformational difference between the two monomers occurs through a rigid body movement involving the long hinge helix (residues 973–992). With respect to monomer-B, the hinge helix in monomer-A is considerably bended and the two GGDEF domains are translated of 22 Å and rotated of 30° with respect to one another (Fig. 5A). The dimeric assembly of DUAL is mainly due to the interaction between the EAL domains, which form the classical dimer observed in other EAL containing proteins [14–17], and in the *P. aeruginosa* homologous hybrid proteins MorA and MucR [4,18]. The interface consists of two antiparallel α-helices making symmetrical contacts and two H-bonds between the backbone of residues belonging to the loop containing the conserved motif DDFGTGYS (residues 1136–1143 in DUAL), involved in allosteric regulation of PDE activity [15,17,19]. An additional salt bridge between His-810 and Glu-925 and a π-cation interaction

Table 1. Kinetic parameters of RmcA constructs and DUAL mutants of c-di-GMP hydrolysis (pH 8.0, 25 °C).

Protein	GTP (μM)	K_M (μM)	k_{cat} (min^{-1})
DUAL	–	4.1 ± 0.4	0.09 ± 0.2
	4	2.5 ± 0.9	0.2 ± 0.1
	8	4.2 ± 1.2	0.3 ± 0.2
	50	2.5 ± 0.5	0.35 ± 0.1
EAL-2		5.9 ± 0.8	0.66 ± 0.2
DUAL E890A	–	11.6 ± 3.5	0.1[a]
	50	9.6 ± 0.1	0.54[a]

[a]To fit these data, the V_{max} parameter has been imposed; this value falls within the range of the V_{max} observed for the wild-type constructs and allowed the best fit of the experimental data. This constraint represents the hypothetical V_{max} of catalysis, if the substrate inhibition does not take place and therefore it represents an extrapolated value. Therefore, it is not a real k_{cat} but an extrapolated V_{max} (with 1 μM enzyme), yielding the K_M values reported in the Table and the following K_i: 10.9 ± 2.2 μM without GTP and 17.8 ± 1.8 μM with GTP. Data fit has been done considering one monomer of the EAL as the active site, to simplify the model, independently on the catalysis occurring on the other monomer of the EAL/EAL dimer; nevertheless, more complex model, involving the EAL dimer, should be also considered for dissecting EAL mechanism [19].

(Phe-927-Arg-874) at the interface between the two GGDEF domains further stabilizes the asymmetric dimer. In the EAL domains, the residues responsible for metal and c-di-GMP binding are conserved and each domain binds one calcium ion in the EAL active site (Fig. 5B). As suggested by structural superposition with homologous domains crystallized in complex with c-di-GMP, only an open conformation of the EAL active site, as seen in DUAL monomer-B, is competent for substrate binding, since the bending of the hinge helix, observed in monomer-A, shifts the α1-helix of 3.1 Å towards the centre of the active site closing the cleft that hubs one guanine of c-di-GMP (Fig. 5B). The asymmetric structure of DUAL, with only one subunit competent for substrate binding (monomer-B) matches the observed stoichiometry of MANT-c-di-GMP binding to DUAL (~ 0.6 molar ratio). As MANT-c-di-GMP is able to fully saturate DUAL in the presence of GTP, the complete conformational transition following GTP binding likely favours the opening of the active site in the EAL domain (monomer-B like conformation). Accordingly, an increase in the DUAL volume in solution upon GTP binding is also observed by Dynamic Light Scattering and Analytical Size Exclusion Chromatography (Fig. 5C).

The dramatic difference in the reciprocal orientation of the GGDEF domain with respect to the EAL domain observed in the asymmetric DUAL structure indicates that the hinge helix allows a great conformational variability to the hybrid domains. In agreement with this observations, the structural superposition of DUAL with the two homologues MorA [4] and RbdA [7] shows not only that the hinge helix is very flexible, but also that the GGDEF domain is able to assume any possible orientation with respect to the EAL domain (Fig. 5D). Therefore, the two conformations observed in the asymmetric dimer of DUAL may represent two intermediate structural snapshots of the events following GTP binding and leading to a fully active ON species. Indeed a large conformational rearrangement upon GTP binding, leading to a more elongated active dimer, has also been proposed for RbdA [7]. The structure of RbdA, encompassing a PAS-GGDEF-EAL construct, was solved as a symmetric dimer, which appeared to be inactive given the separation of the two EAL domains. The results presented so far therefore indicate that GTP binding to the GGDEF domain exerts a dramatic effect also on the overall conformation and function of RmcA DUAL domain.

Analysis of the GTP binding mode in the two GGDEF active sites

One GTP molecule is bound to the active site of the GGDEF domain in both monomers. Together with GTP, one calcium ion is octahedrally coordinated in monomer-B, while two calcium ions are present in monomer-A (Fig. 6A); regardless of metal content, the GTP binding mode is the same in both subunits and similar to that observed in RbdA [7]. With respect to the GTP-αS complexes available [20,21], the position and interaction network of the guanine base of GTP is conserved, while the α-phosphate has a very different conformation. The α-PhO, which in GTP-αS does not bind the metal, is involved in metal coordination in both subunits of DUAL, occupying the sixth ligand position for metal-1 in monomer-B and bridging both metals in monomer-A (Fig. 6A). In the bimetallic site, the two aspartate residues (Asp-889 and 846) that coordinate only metal-1 in monomer-B, bridge both metals. Thus, in monomer-A, the coordination geometry of metal-1 is more distorted than in monomer-B. The glutamate belonging to the GGDEF signature (Glu-890), serves as the fourth ligand of metal-2 in monomer-A, while in the other monomer its side chain is rotated and makes no interactions (Fig. 6A). Finally, the α1-helix of EAL domain in monomer-A is closer to the GTP binding site than in monomer-B (Fig. 6A).

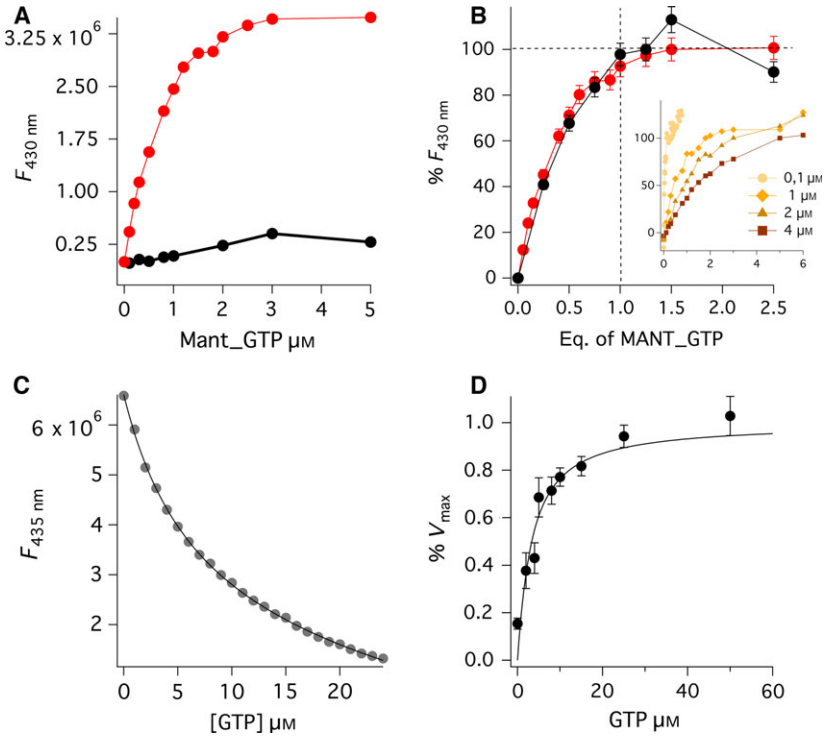

Fig. 3. Binding of GTP to DUAL domain. (A) Comparison of the binding plot of DUAL (red circles) or EAL-2 (black circles) with MANT-GTP. No binding was observed with the latter construct. (B) Titration of DUAL (2 µM) with MANT-GTP (red circles) yields a stoichiometry of 1 GTP:1 DUAL monomer; the same profile was observed in the presence of excess c-di-GMP (30 µM, black circles). On the *Y*-axis is reported the ratio between FRET signal at 430 nm at a given ligand concentration and the plateau value (100% of bound species), considering the plateau value as the *Y*-intercept of the line parallel to *X*-axis fitting the plateau points. Data are the means of two independent experiments and errors (± SD) are within 5%. In the inset the same experiment carried out in the presence of different amounts of protein (0.1, 1, 2 and 4 µM); the value of MANT-GTP required to reach the plateau, and therefore to saturate the protein, depends on the amount of protein. This is typical of a titration plot, where the total ligand added reported in the abscissa axis is approximate to the bound ligand (see Materials and methods for details). (C) Binding of GTP to DUAL (1 µM) assayed by displacement of MANT-GTP. The competition experiment was carried out in the presence of a constant concentration of MANT-GTP (5 µM) and various competitor concentrations (i.e. GTP); buffer conditions are those optimized for PDE activity. The *Y*-axis values are the fluorescence value at 435 nm. Data were fitted (continuous lines) with the displacement equation (see methods), yielding K_{displ} = 6.93 ± 0.4 µM. Data are the mean of two experiments ± SD. At this stage we cannot extrapolate the precise K_D for GTP, since we do not know the exact $K_{D\text{-MANT-GTP}}$. However we can calculate that, since $K_{D\text{-MANT-GTP}}$ is submicromolar, also the corresponding competitor K_D will fall in the same range; as an example, if the $K_{D\text{-MANT-GTP}}$ is 0.1 µM we would have $K_{D\text{-GTP}}$ 0.13 µM (see Materials and methods for calculation details). Given that addition of GTP to DUAL during stirring leads to protein aggregation/precipitation as during an ITC run, this peculiar behaviour hampered ITC experiment with DUAL and GTP, and therefore the precise determination of K_D. (D) PDE activity was assayed with 30 µM c-di-GMP at different GTP concentrations; the $v_{0\ obs}/V_{max}$ ratio as a function of GTP concentration is reported (black circles). Data are the means of three experiments ± SD and were fitted with the reversible binding equation (continuous line).

GTP binding may therefore prime the activation of DUAL to enter PDE catalysis by displacement of EAL (via α1-helix), possibly through the reorganization of the GTP molecule in the binding site, mainly at the level of the α-phosphate. To validate this, we investigated whether the GTP analogue GTP-α-S, whose binding geometry differs from that of GTP (Fig. 6A), triggers PDE activation to the same extent of GTP. As shown in Fig. 6B, the α-substitution abolishes the positive effect of GTP on PDE activity and lowers DUAL affinity for GTP, while the γ-S analogue does not. GTP-α-S does not affect MANT-c-di-GMP binding, whose titration profile resembles that observed in the absence of GTP (Fig. 6C,D). Thus, the α-substitution likely forces GTP in a nonproductive conformation to trigger EAL displacement.

To further probe the environment around the α-bond moiety, we mutated the glutamic acid residue of the GGDEF signature, which, in the closed monomer of DUAL, coordinates metal-2 bridging the α-PhO group (Fig. 6A). The corresponding E890A mutant was characterized kinetically with and without

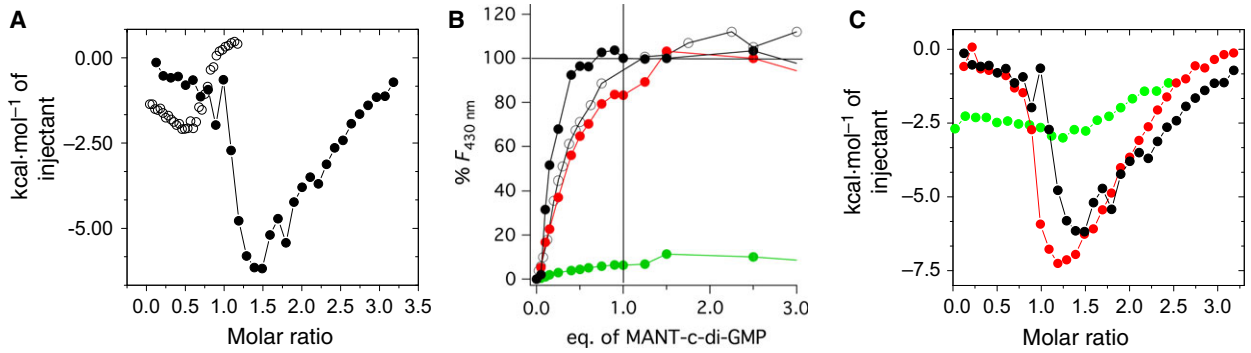

Fig. 4. Interaction of DUAL with c-di-GMP. (A) Binding of c-di-GMP to EAL-2 (open circles) and to DUAL (black circles) was assayed by ITC, at 25 °C, by titrating 35 μM or 25 μM protein with 195 μM or 390 μM c-di-GMP, respectively; the heat exchange/mol of injectant has been reported in the figure and data were fitted with a single binding site equation [according to the ORIGIN (OriginLab Corporation, Northampton, MA, USA) software provided by the vendor]. Data fit parameters for EAL-2 yields a stoichiometry of 0.9 ± 0.2, K_D = 0.17 ± 0.03 μM, ΔH = −3.1 ± 0.6 kcal·mol^{-1}, ΔS = 20.6 ± 1.5 cal·mol^{-1}·deg^{-1}. Data are the mean of three independent experiments ± SD. Titration of DUAL shows a very complicated profile which hampered unambiguous data fit (see Materials and methods for details). (B) Binding of MANT-c-di-GMP to DUAL and EAL-2 (black and empty circles, respectively) assayed by FRET titration of 4 μM protein with different amounts of MANT-c-di-GMP. The titration of DUAL was carried out also after preincubation with 80 μM GTP (red circles); the experiments were repeated twice and variability is within 5%. To probe that MANT-c-di-GMP binds specifically to the EAL active site, MANT-c-di-GMP titration was carried out also with the DUAL double mutant D1136N-D1137N (hereinafter DUAL_DD), in which the double mutation hampers the metal-dependent binding of c-di-GMP to the EAL active site. As expected, no significant binding is observed (green circles, normalized according to 100% observed with wild-type DUAL). (C) Binding of c-di-GMP to DUAL as assayed by ITC. In the figure, plot of the heat exchange (per mol of injectant) observed upon titration of 25 μM DUAL (in the cell) with 390 μM c-di-GMP (in the syringe), with or without incubation with 50 μM GTP (red and black circles, respectively). ITC on DD-DUAL (green circles), which is not able to bind c-di-GMP in the EAL active site, suggested that low-affinity binding events are still present; possibly it could represent a residual binding to the mutated EAL site.

GTP. Contrary with the wild-type protein, the dependence of v_0 on substrate concentration yields a bell-shaped curve, indicative of substrate inhibition (Fig. 7A), with a K_i for c-di-GMP close to the apparent K_M (17.8 *vs* 9.6 μM, in the presence of GTP) (Table 1). The mutant still responds to GTP (Table 1), but above 10 μM c-di-GMP, E890A is not able to sustain the activation triggered by GTP and PDE turnover drops dramatically ~ 100 s after substrate addition (Fig. 7B). As shown above, binding of GTP to the wild-type DUAL protein affects c-di-GMP binding to EAL: this effect is abolished by the E890A mutation (Fig. 7C). This behaviour is not due to changes in GTP affinity, which is not significantly altered in the mutant (Fig. 7D,E).

We propose that the effect of the E890 mutation at the level of the GGDEF domain is propagated to the EAL/EAL interface, thereby altering the PDE kinetic profile, resembling the profile previously observed for mutants located at the dimerization interface of other EAL PDEs. In the case of these mutants, binding of c-di-GMP to one monomer fails to induce the proper conformational change (linked to the coordination of a second metal ion in the EAL binding site) of the conserved DDFGTGYS motif; thus c-di-GMP bound to one monomer negatively affected the catalytic efficiency of the other EAL monomer resulting in a substrate inhibition profile [17,19]. Observing a similar profile for the E890 mutant is the first evidence of a mirroring effect on an hybrid domain, i.e., a mutation in the GGDEF signature able to affect the EAL/EAL crosstalk, resulting in uncoupling of GTP binding and PDE activation. Moreover, the catalytic profile of this mutant suggests that the EAL/EAL dimerization is one of the step of the GTP-dependent protein activation.

Hypotetical allosteric model of GTP-dependent activation of RmcA

As already mentioned, our biochemical data suggest that DUAL populates at least two distinct conformational states that are associated with low and high PDE activities. The different bending of the hinge helix between the two DUAL monomers (Fig. 5A) suggests that the ON→OFF switch may involve the transition from an elongated to a more compact conformation, resulting in a closer contact between the EAL and GGDEF domains. Therefore, starting from our structural data and from the structure of the homologous protein MorA (~ 65% sequence identity; [4]), we speculated on two plausible models of the fully

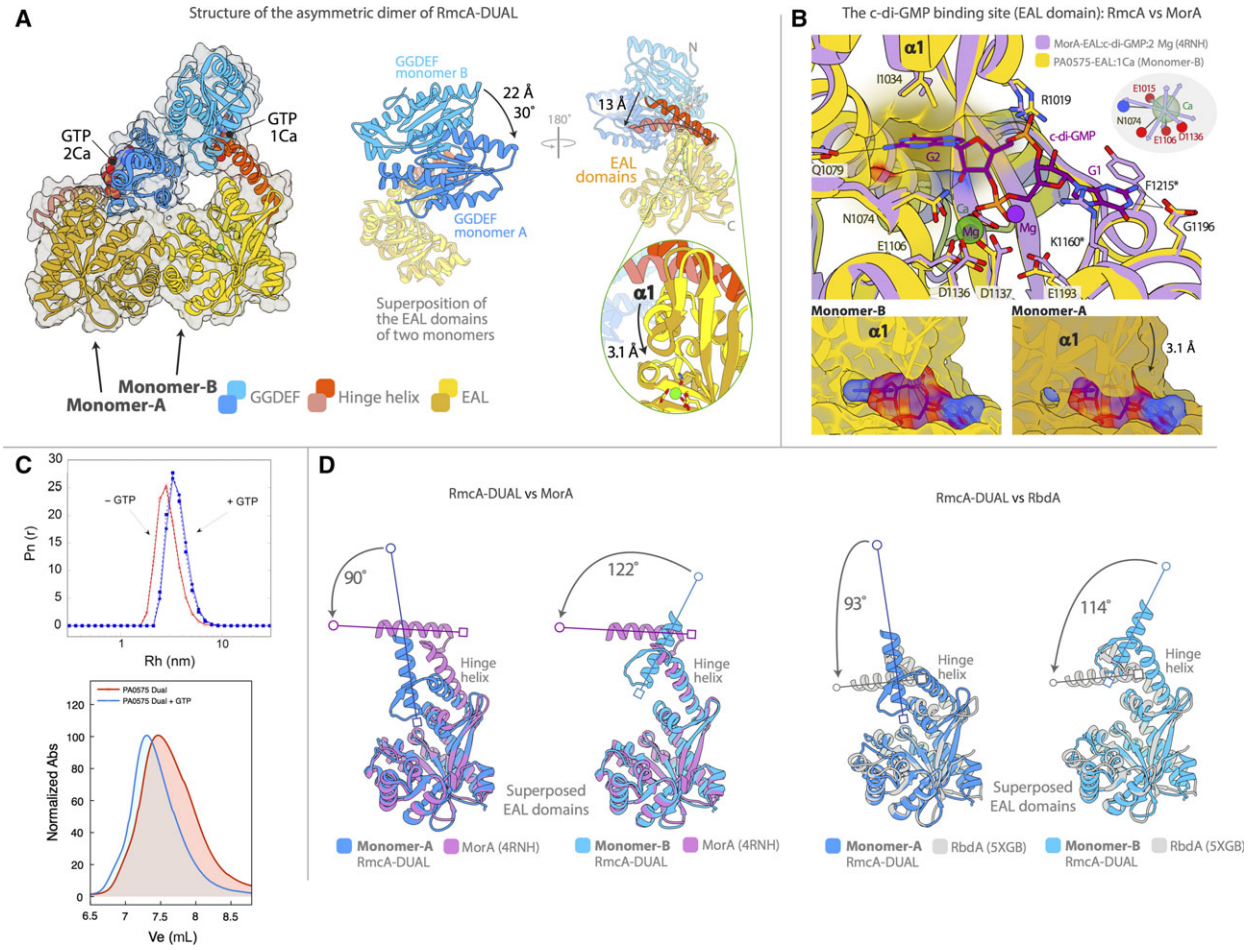

Fig. 5. Structure of RmcA-DUAL. (A) On the left: structure of the asymmetric dimer. In each monomer the N-terminal GGDEF (blue), the connecting helix (red) and the EAL domain (yellow) are highlighted in different colours. The GTP molecules and calcium ions are shown as spheres. In the centre and right side: superposition of the EAL domains of the two monomers showing the conformational differences in the relative orientation of the GGDEF domain with respect to the EAL domain. The bending of the connecting helix and the corresponding shift of helix α1, belonging to the EAL domain, is highlighted in the blow-up. (B) Top; the c-di-GMP binding site. Superposition of the EAL domain of RmcA-DUAL (monomer-B, yellow) with the homologue hybrid protein from *Pseudomonas aeruginosa* MorA in complex with c-di-GMP and 2 Mg^{2+} ions (4RNH, violet) [4]. Residue numbering refers to RmcA. Two side chains that were not visible in the electron density and are marked with an *. C-di-GMP is harboured in the EAL active site by multiple interactions. One guanine (G2) docks in a hydrophobic cleft flanked by helix α1. In monomer-B the 3.1 Å shift of this helix seals the cleft, making c-di-GMP binding impossible, as shown in the bottom panels by surface representation of the hydrophobic cleft harbouring guanine G2. The cleft is well accessible in monomer-B (lower left) and closed by the helix α1 shift in monomer-A (right). (C) Upper panel. Dynamic light-scattering measurements. Hydrodynamic radius (Rh) and number distribution (Pn) of the 4 μM protein in the PDE buffer, both in the absence and in the presence of GTP at a final concentration of 50 μM; the hydrodynamic radius of DUAL in the presence of GTP increases from 2.96 to 3.6 nm, leaving substantially unchanged the polydispersity index. Lower panel. Size-exclusion chromatography on a HPLC G3000PWXL colunm, 0.8 $mL \cdot min^{-1}$. Chromatographic profiles of DUAL samples eluted ± GTP (blue and red line, respectively); GTP yields a population of DUAL (GTP-bound) with a significantly higher hydrodynamic volume than the GTP-free counterpart. (D) Structural comparison of monomer-A and B of DUAL with the monomers of the homologues MorA (4RNH) and RbdA (5XGB). Given the very different conformations, only the EAL domains were superposed. To show the different orientations of the GGDEF domains with respect to the hinge helix only the last (C-terminal) α-helix of the GGDEF domain is shown. An indication of the orientation of this helix is also added for clarity, with the square end corresponding to the connecting of the GGDEF domain with the hinge helix (C-terminal of the GGDEF domain). The very different angles account for the difference in the orientations of the GGDEF domains among the superposed structures.

ON and OFF conformations of RmcA, which could also be compatible with the full-length protein. These hypothetical models were constructed in an attempt to locate the conformational hot-spots of RmcA.

In modelling an ON symmetric dimer of DUAL, we initially compared the two DUAL monomers with MorA. Both MorA and monomer-B of DUAL appear to adopt an 'open' conformation, with the hinge helix connecting the GGDEF and EAL domains being completely 'straight', and spatially separating, in this way, the GGDEF from the EAL domains. Moreover, we observed that the single EAL domains of monomer-B and MorA superposed very well (RMSD < 1.0 Å), while the GGDEF domain shows a 120° torsion in monomer-B with respect to the same domain of MorA (in spite of the fact that the single GGDEF domains are also very similar, with a RMSD < 1.0 Å) (Fig. 5D). Since an hypothetical symmetric dimer with both subunits in the conformation of monomer-B is incompatible with the upstream LOV domain in the full-lenght RmcA protein, we modified the orientation of the GGDEF domain of the DUAL monomer-B, to resemble the GGDEF-EAL orientation observed in MorA [4]. Notably, in this hypothetical symmetric model the orientation of the N-terminal GGDEF tails would be compatible with the upstream LOV domain C-terminal tails, as observed in the crystal structures of LOV domains retrieved from PDB (data not shown) (Fig. 8A,B). Moreover, this assembly of the GGDEF domains also coincides with the catalytically inactive conformation of previously solved GGDEF domains [22], which shows no detectable c-di-GMP cyclase activity.

On the other hand, monomer-A of DUAL, displaying a more compact conformation, was used as a starting point to model an OFF state of RmcA. To this aim, we investigated the ability of monomer-A to reach a fully closed state, performing an all-atom normal mode (NM) analysis (Movies S1 and S2; [23,24]). NM motions described by the lowest frequency Normal Mode suggest that indeed monomer-A of DUAL is able to adopt a fully closed OFF state (Fig. 8A,C), in which the α1-helix of the EAL domain is very close to the GTP binding site of the GGDEF domain. Notably, the NM data also corroborates the high flexibility of the GGDEF-EAL domains interface inferred from crystallographic B factors of monomer-A. Albeit it was not possible in the latter case to obtain a symmetric dimer of the OFF state, we expect that in such state the EAL domains would be 'locked' in a confirmation that prevents their dimerization, via close contacts involving residues of EAL and GGDEF domains, as observed in other GGDEF-EAL structures [7,25].

Comparing the obtained OFF and ON models, we confirmed that the α1-helix of the EAL domain in monomer-A is closer to the GTP binding site than in monomer-B (Fig. 8C), suggesting that GTP binding may prime the reorganization of the GTP neighbouring residues in the binding site and drive the conformational OFF→ON transition. Moreover, we noticed that the invariant residue Arg980 (according to the multiple sequence alignment of ~ 250 protein homologues of PA0575; data not shown), which is located at the centre of the hinge helix connecting the GGDEF and EAL domains, participates in contacts with both the GGDEF and EAL domains, thus bridging their interactions only in the OFF state (Fig. 8C). We therefore hypothesized that, upon GTP binding, a rearrangement of the Arg980-mediated GGDEF-EAL domains interactions could destabilize the OFF state and favour the opening of the DUAL module, through the unbending of the hinge helix. Interestingly, Arg980 is proposed to stabilize also the ON state, due to its electrostatics interactions with residues Glu1038 and Asp1039 of the EAL domains (Fig. 8B). Thus, GTP is proposed to 'unlock' the EAL domains and to allow, through a large conformational change in the hinge helix, their dimerization and subsequent activation (Fig. 8A).

To corroborate this mechanistic model, we mutated the Arg980 residue, which is likely involved in stabilizing both the OFF and the GTP-derived ON conformations. We found that the PDE activity of the corresponding R980S mutant becomes GTP-independent, and significantly higher than that of the GTP-free wild-type (Fig. 8D). Therefore, the substitution of this residue appears to uncouple GTP binding and protein activation. While the OFF→ON equilibrium of wild-type DUAL, as purified in the absence of GTP, is largely shifted towards the OFF state, in the presence of the Arg980Ser mutation such equilibrium switches to favour the ON state, likely by promoting the conformational transition required for PDE activation via OFF destabilization. On the other hand, it must be noted that the observed activities are slightly slower than the activity of the wild-type protein in the presence of GTP (Fig 8D). This could be due to the fact that, according to the model, Arg980 makes electrostatic interactions with Glu1038 and Asp1039 in the ON state, thus also contributing to stabilize the ON conformation. However, the latter effect is perhaps of secondary importance if compared to the ability of Arg980 to 'lock' the OFF state. To validate this hypothesis, we mutated the counterpart of this hypothetical interaction (E1038A/D1039A double mutant). As expected, the activity of this double

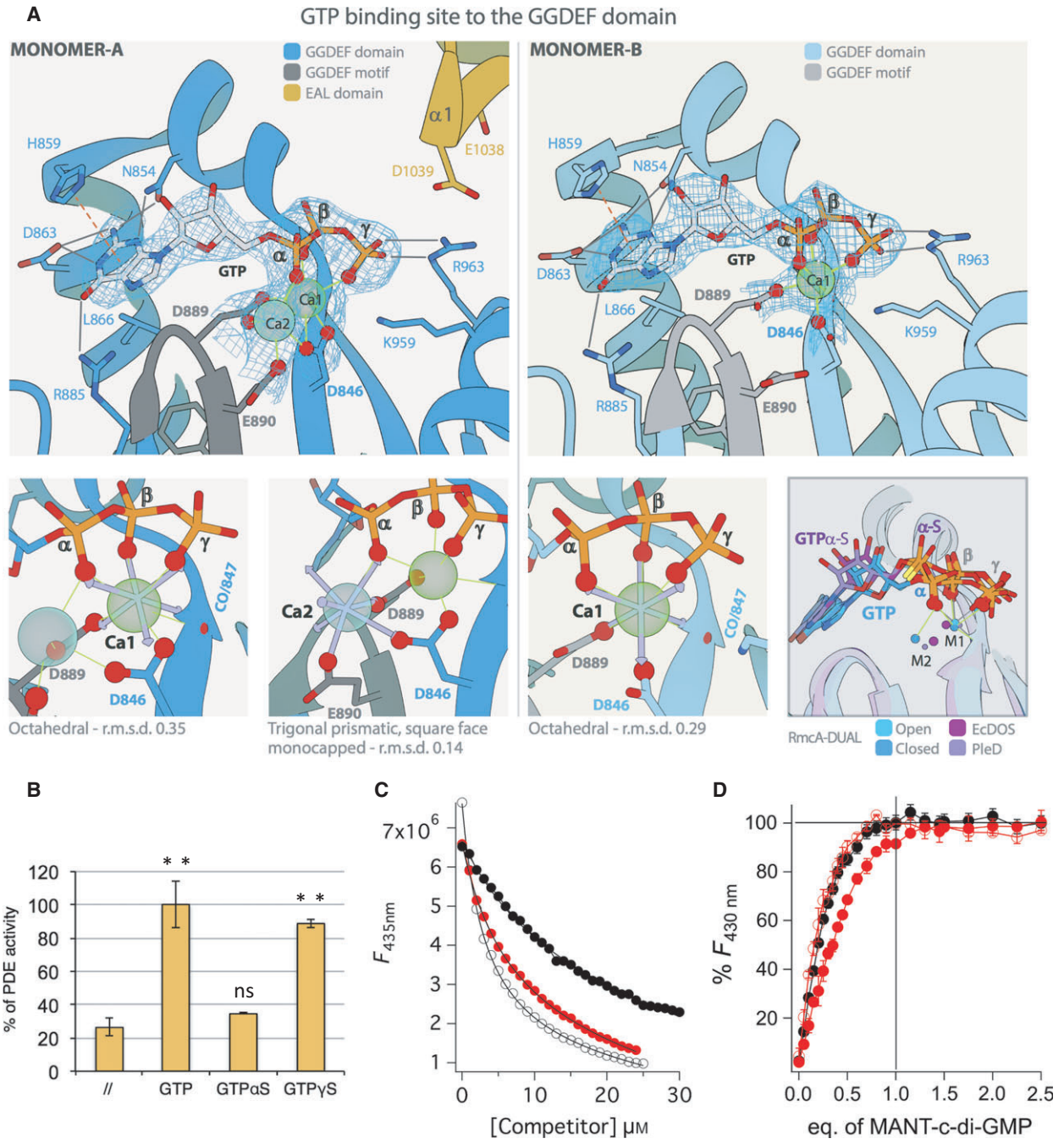

mutant, in the presence of excess GTP, superposes with that of R980S mutant being also in this case slightly lower than that observed in the GTP-containing wild-type protein. Interestingly, in the absence of GTP the activity of the E1038A/D1039A double mutant is dramatically affected by the mutation, being ~ 5-folds lower than the wild-type. This indicates that this double mutation affects the OFF→ON equilibrium found in the 'as purified' wild-type protein, increasing the population of the OFF form. Taken together, these results strongly indicate that Glu1038 and Asp1039 are involved in stabilizing the fraction of protein in the ON state, likely via their interaction with Arg980. In the double mutant, Arg980 loses its contact(s) in the ON conformation, while it is still able to stabilize the OFF state, thus accounting for the poor basal catalytic activity of the E1038A/D1039A double mutant.

Fig. 6. GTP binding to the GGDEF domain. (A) GTP bound to the GGDEF domain in monomer-A (left) and to monomer-B (right). Electron density maps ($2F_o-F_c$) for GTP, Ca^{2+} ions and coordination atoms are shown with a contour level of 1.3 σ. Residues belonging to the GGDEF motif are coloured in grey. Monomer-A contains two calcium ions (Ca1 and Ca2), while in monomer-B only one ion is observed, in the same position corresponding to Ca1. The coordination geometry of the metals is highlighted in the boxes below. The three phosphates of GTP, Asp-864, the main chain oxygen of Leu-847 and Asp-889 (belonging to the GGDEF motif) function as ligands of the octahedrally coordinated Ca1 in both monomers, with a RMSD from ideal geometry that is lower in monomer-B. The second calcium ion (Ca2), present in monomer-A, is coordinated by four out of seven ligands necessary to complete the trigonal prismatic coordination geometry. Three of these residues bridge both metals (α-PhO; Asp-864 and the GGDEF Asp-889), while the fourth additional ligand atom is provided by the glutamate of the GGDEF signature (Glu-890). The bottom-right box shows the different binding mode of GTP-αS (as observed in *Caulobacter crescentus* PleD – 2V0N-[21] and *Escherichia coli* DOS – 4ZVF- [20]) with respect to GTP. The presence of the sulphur atom does not allow the α-PhO to coordinate the metal in position 1. (B) PDE activity of DUAL (1 μM) at 30 min after substrate addition carried out with 30 μM c-di-GMP and, when indicated, with either 50 μM GTP or GTP-α-S or GTP-γ-S (at RT); pGpG content was determined by RP-HPLC. Activity observed with GTP was considered as reference of maximal activity (100%), as compared to the other samples. Data are the means of at least two experiments ± SD. Statistical significance for each construct with respect to the assay without GTP is indicated (** in the figure), being $P < 0.01$; ns: not significant. Not significant differences are observed between the assay with GTP and its analogue GTP-γ-S ($P = 0.25$). (C) Binding of GTP and its analogues to DUAL (1 μM) assayed by displacement of MANT-GTP. The competition experiment was carried out in the presence of a constant concentration of MANT-GTP (5 μM) and various competitor concentrations (i.e. GTP-γ-S, empty circles; GTP-α-S, black circles and GTP, red circles for comparison); *Y*-axis values are the fluorescence at 435 nm. Data were fitted (continuous lines) with the displacement equation, yielding K_{displ}: 3.3 ± 0.1 μM for GTP-γ-S; 14.6 ± 0.6 μM for GTP-α-S. Data are the mean of two experiments ± SD. Accordingly, the affinity scale is: GTP-γ-S> GTP> GTP-α-S. (D) Titration of DUAL (2 μM) with different amounts of MANT-c-di-GMP in the presence of 50 μM GTP-α-S (black circles) is compared with the experiments carried out with or without 50 μM GTP (red and empty circles, respectively). Data are the mean of three independent experiments ± standard deviation.

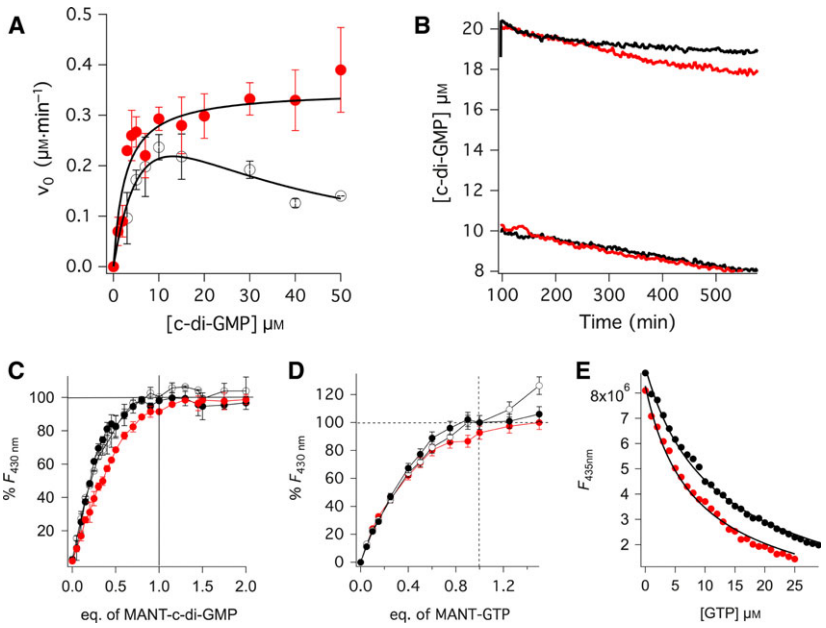

Fig. 7. Characterization of the E890A mutant. (A) The initial rate of PDE kinetics of E890A carried out in the presence of excess GTP (50 μM) was plotted as a function of c-di-GMP concentration and compared to that of DUAL (empty and red traces, respectively). In the case of the mutant, data were fitted with substrate inhibition equation. Data are the means of three independent experiments ± SD. (B) Time-course of PDE kinetics obtained at 10 and 20 μM c-di-GMP, 1 μM protein (E890A in black, wild-type in red). (C) Interaction of E890A with c-di-GMP was investigated by titrating 2 μM of protein with different amounts of MANT-c-di-GMP, both in the presence or in the absence of excess GTP (50 μM, black or empty circles, respectively); the presence of GTP does not increase the equivalents of MANT-c-di-GMP bound, as observed in the wild-type protein (red circles). Data are means of three independent experiments ± SD. (D) Interaction of E890A with GTP was investigated by titrating 2 μM of protein with different amounts of MANT-GTP (black open circles). The titration profile superposes with that of the wild-type protein (red circles); the same profile was observed in the presence of excess c-di-GMP (30 μM, black circles). Data are the means of at least two independent experiments and errors (± SD) are within 5%. (E) Competition experiment of MANT-GTP with GTP, carried out on E890A (in black, as compared to the wild-type, in red). Data fit yields a K_{displ} = 10.6 ± 2.2 μM.

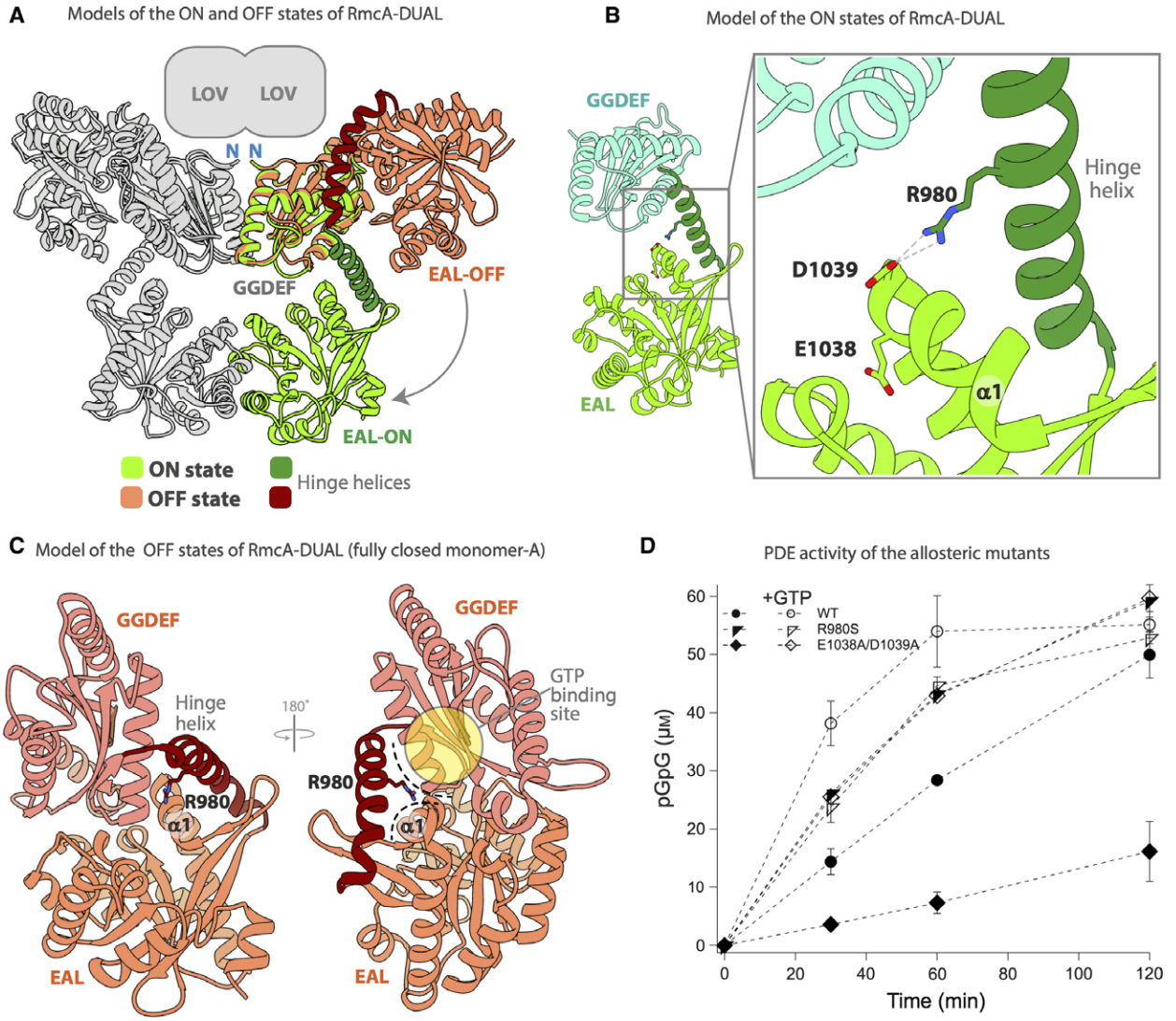

Fig. 8. GTP-dependent PDE activation. (A) Comparison of the symmetric dimers of the ON model (derived form the structure of MorA [4], green) and the OFF model obtained by NM analysis starting from the structure of monomer-A (orange). Notice that the GGDEF domains were oriented as in the structure of MorA in order to be compatible with the upstream LOV domains. The GGDEF domains of the two models are superposed to show the different orientation of the EAL domains. (B) Model of one monomer in the open (ON) conformation. The hinge helix is in an elongated conformation separating the GGDEF from the EAL domain, which can thus forms the classic dimer (competent for catalysis). In this ON conformation Arg980 is in close contact with both Asp1038 and Glu1039. (C) Model of one monomer in the closed (OFF) state. The GGDEF and the EAL domains are in close proximity and Arg980 makes contacts with both the GTP binding site (highlighted) and the EAL domain at the level of α1. (D) PDE activity of 10 μM wildtype (circles), R980S (triangles) and E1038A/D1039A (diamonds) DUAL carried out in the presence of 60 μM c-di-GMP as substrate with or without 100 μM GTP (empty and black simbols, respectively). Nucleotide content of each mixture was assayed by RP-HPLC after 30 min of reaction at 25 °C. Data are the mean of at least two experiments ±SD.

Discussion

Our results show that the *P. aeruginosa* PAO1 multidomain protein RmcA, which we recently found to respond to the nutrients status by lowering c-di-GMP levels *in vivo* [10], is a GTP-dependent PDE.

We found that in RmcA DUAL, binding of GTP to the GGDEF releases the negative control of this domain on the EAL one; additionally, structural and protein engineering data suggest that GTP binding to the GGDEF domain of RmcA affects the assembly of EAL domains, likely by displacing the α1-helix and reorganizing the hinge helix, thereby promoting/stabilizing EAL-EAL dimerization. Since c-di-GMP binding to the EAL active site is known to stabilize the

EAL/EAL interface [19], it is likely that, once GTP has triggered the transition, c-di-GMP is also required to fully stabilize the ON state (Fig. 9 for a summary of the proposed mechanism).

The GTP-dependent allosteric control of the GGDEF domain over the EAL domain was already described for other hybrid proteins [6,26] (Table S2); Christen *et al.* suggested that under physiological conditions the GTP-dependent PDE activity of the hybrid protein CC3396, a GGDEF-EAL protein from *C. crescentus*, could be maximal given that GTP is saturating. They also proposed that uncontrolled PDE-dependent decrease in c-di-GMP levels could lead to the activation of those DGCs negatively controlled by c-di-GMP and finally to possible GTP depletion; nevertheless, if GTP is the modulator of the c-di-GMP consumption rate by DUAL-like PDEs, the risk of nucleotide unbalancing is lessened [5]. The concentration of c-di-GMP could be very different in cell, being in the low μM range [27–29] (with a 100 : 1 ratio with GTP [30,31]), This ratio (GTP:c-di-GMP) reportedly could be reverted into 1 : 10 once c-di-GMP levels increase for DGC over-expression, being GTP pool depleted only for 30%, thus confirming that fine tuning of GTP levels takes place [30].

It should be mentioned that, under stress conditions and nutrients starvation, GTP pool could dramatically drop (by a factor of 5; [32,33]) through the conversion of this nucleotide into (p)ppGpp [34,35]. Therefore, the GTP-dependent control of PDE activity could also be a strategy to promote the decrease in c-di-GMP levels (and the related phenotypes such as biofilm dispersion) only under maximal biosynthetic potential (known to be linked to high GTP levels).

As already mentioned, the obtained results demonstrate that GTP affects RmcA in the micromolar range, which is much smaller compared to the millimolar range of GTP levels in live cells. In this scenario, therefore, under not stringent nutrient conditions, the GTP-binding site of GGDEF would always be fully occupied by GTP, precluding any regulatory role of the latter. Actually, this apparent conundrum could be

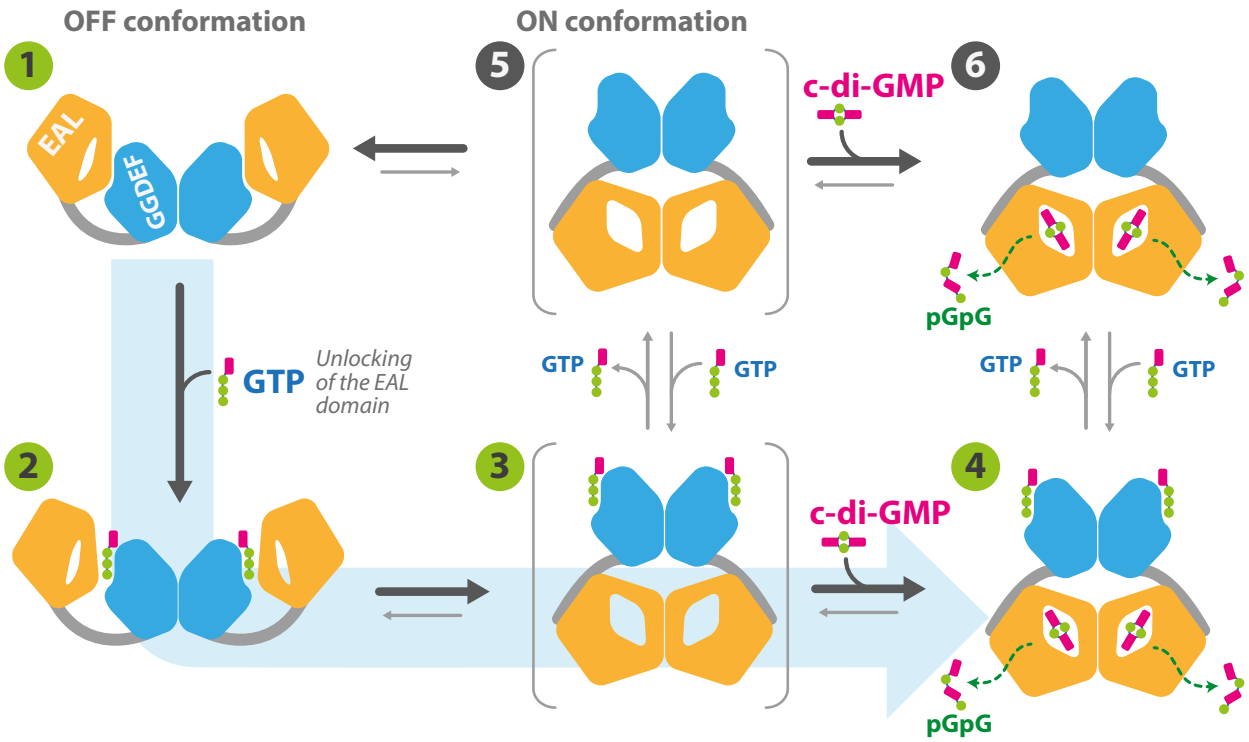

Fig. 9. Proposed mechanism of RmcA activity. In this scheme, the various species involved in the activity are depicted and numbered progressively. Species 1 represents the starting OFF conformation: this is converted into species 2 by GTP binding, which drives unlocking of the EAL domains (likely in equilibrium with species 3). Binding of c-di-GMP to species 3 (at the EAL active site) populates species 4, which represents the PDE-active cycling species. Thus, in the presence of c-di-GMP, the equilibrium is shifted towards species 4 along the blue pathway. In solution, species 1 is likely in equilibrium with a small fraction of species 5, which is able to react with c-di-GMP, yielding the observed basal PDE activity without GTP (species 6). The K_D for GTP obtained from data reported in Fig. 3D likely accounts for the equilibrium between species 3 and 5.

addressed by acknowledging the possible *in vivo* modulating roles of the upstream domains of RmcA that are missing in our construct on the Kd for GTP and/or the organization and oligomeric state of the GGDEF-EAL module.

In line with this, we recently found that RmcA is an Arginine sensor [10] via its periplasmic domain, able to decrease c-di-GMP intracellular levels in response to this nutrient.

Moreover, domain composition analysis of RmcA (data not shown) suggests that residues 677–795 constitute a Light, Oxygen or Voltage (LOV) domain, belonging to the PAS superfamily, upstream the GGDEF-EAL dual structure. Interestingly, LOV domains are known to make use of a flavin cofactor (FMN or FAD) to sense light, redox or voltage modifications, regulating the activity of their adjacent domains in response to such changes. In response to a signal, as noted by Key *et al*. [36], the prompt reorganization of FMN/FAD hydrogen-bonding network leads to a conformation change in an N- and/or C-terminal helix that lies adjacent to the PAS/LOV domain core. It is interesting to note here that, according to this model, if such conformational rearrangement takes place, it could affect also the relative orientations of the GGEDF domains downstream the helix of the RmcA LOV domain.

Therefore, modifications of the redox state of FAD in the LOV pocket, rather than or in addition to GTP binding to the A site of the GGDEF domains, could lead to the release of the autoinhibitory interactions of RmcA, allowing the GGDEF and EAL domains to rearrange into a canonical dimer capable of hydrolysing the incoming c-di-GMP substrate, as observed in MorA [4]. In agreement with this view, in PA14 strain, the homologous RmcA protein contains FAD in the cytoplasmic portion and responds to phenazines [12].

The multilevel control of c-di-GMP levels has been acknowledged very recently by the O'Toole group [37]; in this study, the authors clearly demonstrate that nutrients are the driving force of the global c-di-GMP-related metabolism and the sensing mechanism mainly involves allostery rather than other regulatory mechanisms.

We propose that detection of Arginine by the periplasmic sensor domain of RmcA leads to a conformational rearrangement of the bundle of TM helices and of the PAS/LOV helices. This observation would lead to the interesting hypothesis that RmcA and its homologous proteins function as 'rheostats', by integrating Arginine signals from their periplasmic sensor domains and the general redox state of cell through its LOV domain, with all these signals leading to a contextually optimal PDE activity, mediated by GTP. To shed light on such complex scenario, future studies on RmcA will be required to fully understand the molecular mechanism transducing nutrient sensing into the activation of the GGDEF-EAL effector domains via the PAS/LOV domains, and the eventual involvement of redox components, as recently suggested [12]. It would be exciting to mechanistically demonstrate that RmcA is able to function as a multilevel antenna receptor, which monitors the environment (i.e. nutrient) and the intracellular status (i.e. redox power via flavin/phenazines and general metabolism via nucleotides): this multilayer control allows the bacterium to modulate c-di-GMP to finally direct the cell fate.

Materials and methods

Protein expression and purification

The different constructs of RmcA were obtained by PCR of a synthetic construct of RmcA (GeneArt) encoding for the last 554 amino acid residues and subcloned as N-terminal His-tag constructs in Pet28b (see Fig. 1A for details). Site-directed mutants were obtained using the Quikchange Lighting kit (Agilent Technologies, Santa Clara, CA, USA). All proteins were overexpressed in the *Escherichia coli* BL21 (DE3) strain. Bacterial cultures were grown at 37 °C in Luria-Bertani (LB) liquid medium supplemented with 30 $\mu g \cdot mL^{-1}$ Kanamycin (Sigma-Aldrich, St. Louis, MO, USA) until OD600 $\sim$ 0.8, and then at 20°C for 20 h after addition of 0.5 mM IPTG (isopropyl B-D-thiogalactoside; Sigma). Cells were harvested by centrifugation and bacterial pellets were suspended in lysis buffer (250 mM NaCl, 50 mM Tris-HCl pH 8, 1 mM PMSF and 1 complete protease inhibitor; Roche, Basel, Switzerland) and lysed by sonication on ice. Cell lysate was centrifuged 30′ at 11 800 ***g*** and supernatant purified by IMAC using a Ni^{2+}-HisTrap column (GE Healthcare, Chicago, IL, USA) in buffer A (20 mM Tris-HCl pH 7.6, 150 mM NaCl). Elution was carried out increasing the imidazole concentration, with the protein eluting at 200 mM imidazole. Fractions containing pure protein were pooled and imidazole was removed with PD-10 desalting columns (GE Healthcare). For crystallography, His-tag was removed with Thrombin (Sigma) (5 $U \cdot mg^{-1}$ of target protein), at RT overnight; His-tails were removed by a second HisTrap column, were protein was recovered in the 20 mM eluate. In both cases (with or without His-tag) all the proteins were loaded on an FPLC column (Superdex 200 26/600; GE Healthcare) and eluted with buffer A.

X-ray crystallography

Crystals of DUAL without his-tag were grown at 21 °C by hanging drop vapour diffusion method mixing equal

volumes (1.0 μL) of protein solution – 3 mg·mL^{-1} (60 μM) in 150 mM NaCl, 20 mM Tris-HCl pH 7.6, 2.5 mM $CaCl_2$ and 320 μM GTP (GE Healthcare) – and reservoir – 0.1 M KCl, 10 mM $CaCl_2$, 50 mM sodium cacodylate pH 6.0, 1–2% w/v PEG 3350. Crystals were cryo-protected by soaking in the mother liquor containing 20% v/v glycerol before flash freezing in liquid nitrogen. Diffraction data have been collected on BL14.3 operated by the Joint Berlin MX Laboratory at the BESSY II electron storage ring (Berlin-Adlershof, Germany) [38]. Data were processed using XDS [39] and scaled using Pointless and Aimless in the CCP4 suite [40]. Initial phases were obtained by molecular replacement with Phaser [41] using the GGDEF domain of YfiN (PDB id: 4IOB) [42] and the monomeric EAL domain from MorA (PDB id: 4RNI) [4] as search models. Model building and refinement was carried out with Coot [43] and Refmac5 [44] using ProSMART to generate secondary structure restraints [45] and a 3.0 weight to restraint all geometric parameters. Residues from 809 to 1231, GTP and calcium ions were clearly visible and modelled unambiguously in the electron density. Final statistics are reported in Table 2. The coordinates and structure factors have been deposited in the protein data bank, with accession number: 5M3C.

Table 2. Data collection and structure refinement statistics

	$RmcA^{GGDEF-EAL}$ (DUAL)
Data collection	
Space group	$P2_12_12$
Cell dimensions	
a, *b*, *c* (Å)	122.3, 133.9, 69.1
Resolution (Å)	48.1–2.8 (2.95–2.80)[a]
CC(1/2)[b]	99.8 (74)
Mean $I/\sigma I$	14.6 (2.1)
Completeness (%)	99.9 (99.7)
Redundancy	8.1 (8.4)
Molecules/AU (% solvent)	2 (55)
Refinement	
Resolution (Å)	48.1–2.80
No. reflections	27 257
R_{work}/R_{free}	24.7/27.4
N. atoms/mean *B*-factors (Å^2)	
Protein	6413/64.4
GTP	64/59.3
Ca^{2+}	5/50.7
Water	15/42.1
R.m.s. deviations	
Bond lengths (Å)	0.019
Bond angles (°)	1.997
Ramachandran (*N*/%)	
Favoured	796/94.8
Allowed	42/5
Disallowed	2/0.2

[a]Values in parentheses are for highest-resolution shell. [b]Percentage of correlation between intensities from random half-data sets.

Kinetic assays

All the kinetic assays have been done in 20 mM Tris-HCl pH 8.0, 100 mM NaCl and 2.5 mM $MnCl_2$, using the His-tag containing protein, except for special cases detailed in the figure legends. If indicated, PDE activity was evaluated by reverse-phase high-performance liquid chromatography (RP-HPLC). Briefly, 150 μL of reactions were stopped with EDTA and nucleotide-extracted as described in Ref. [46] at selected times. The reactions products were separated as previously described [13]. Data are the mean of at least two experiments ± SD. Protein and substrate concentrations are detailed in the corresponding figure legends.

Real-time kinetics of PDE activity were assayed by circular dichroism (CD), as previously published [47]. Briefly, protein solution (1 μM) was incubated 10′ at 25 °C; if indicated, the mixture was further incubated 5′ at 25 °C with GTP prior the addiction of c-di-GMP; the reaction was carried out in 1-cm path quartz cuvette in 800 μL of final volume and followed for 10 min. C-di-GMP degradation was monitored following the CD signal at 282 nm, using a JASCO J-710 spectropolarimeter at 25 °C. The values are the means of data from at least three independent experiments, and the errors are ± SD. The c-di-GMP content was extrapolated by using the calibration curve of c-di-GMP previously obtained. These data were used for the Michaelis–Menten plot.

Homology Modelling and NM analysis

The program PHYRE2 [48] was used to detect structural homologues of RmcA (GI: 686131882). The best hit, i.e., MorA (PDB id: 4RNI) [4] was chosen for ON model construction, using PYMOD 2.0 [49,50]. To this end, the GGDEF, hinge helix and EAL domains of the crystal structure of DUAL were initially splitted, and superposed to MorA (RMSD < 1.0 Å). Then, the sequence of RmcA was aligned to MorA, using the programs Muscle [51], PhD server [52] and SCR find [53]. Afterwards, the Modeller package [54] was used to impose hard spatial restraints to keep the structures of the single GGDEF and EAL domains of DUAL, while modelling the ON state according to the domains orientation of MorA. PYMOD 2.0 was used for the manipulation of alignments and to merge the predicted models in a multidomain model. Finally, protein symmetric dimeric models were constructed using the Modeller package [54], and analysed with Dope Score and Verify_3d [55] to monitor their stereochemical quality.

To further investigate the closed state of DUAL, an anisotropic network model was used for Normal Mode (NM) analysis of the monomer-A of DUAL. This approach is usually useful to probe large-amplitude motions, which are often inaccessible to other atomistic

simulations. NM analysis is insensitive to the presence of small molecules, such as GTP, in the context of large-protein systems. Each residue was represented by one bead in its α-Carbon position. These beads were then connected by elastic springs if the distance between two beads fall under a 10 Å cut-off value. The elastic network model was built with PyANM [56] and rendered with PYMOL (Version 2.0 Schrödinger, LLC, Cambridge, MA, USA). The harmonic fluctuations of the first not-trivial NM were then used to further analysis.

Data fit of PDE activity

Since the PDE activity with 50 μM GTP is comparable to that observed in the presence of 80 μM GTP used for the pilot assay, the optimization and the determination of kinetic parameters were carried out in the presence of 50 μM GTP. For Michaelis–Menten plot of DUAL the canonical equation was used, while for E890A fit of kinetic data were carried out with the substrate inhibition equation, using a simple model where binding of a second molecule of substrate to the Michaelis–Menten complex yields a dead-end state:

$$V_0 = \frac{\frac{V_{max}}{1+\frac{[S]}{K_i}} * [S]}{\frac{K_m}{1+\frac{[S]}{K_i}} + [S]}$$

PDE initial rates in the presence of 30 μM c-di-GMP as a function of GTP were fitted with the binding equilibrium equation:

$$fV_{max} = \frac{1 + [\mathrm{GTP}] + K_D - \sqrt{(1 + [\mathrm{GTP}] + K_D)^2 - 4 * [\mathrm{GTP}])}}{2}$$

Binding of fluorescent nucleotide analogoues

Titration of RmcA constructs with MANT-GTP and MANT-c-di-GMP (Life Technologies, Carlsbad, CA, USA) was assayed on a Fluoromax single photon counting spectrofluorometer (Horiba JobinYvon). Briefly, protein tryptophans were excited at 280 nm and the fluorescence emission spectra were recorded between 400 and 550 nm, as a result of Förster resonance energy transfer (FRET) to MANT-GTP or MANT-c-di-GMP (in 1 cm light path; Hellma GmbH & Co. KG, Mullheim, Germany), after 3 min of incubation with the fluorophore. The binding of the phorophores with each proteins was tested in 20 mM Tris-HCl pH 7.6, 150 mM NaCl and 2.5 mM $CaCl_2$ at 25 °C in a final volume of 500 μL. FRET experiments were performed titrating 2 μM of each proteins with MANT-GTP or MANT-c-di-GMP at different concentrations. The binding curve obtained is typical of a titration plot, where the total ligand added reported in the abscissa axis is approximate to the bound ligand; this implies that the K_D for the binding event should be lower than the concentration of the protein assayed (we assayed as lowest [DUAL] 0.1 μM, based on the sensitivity of the technique under these experimental conditions). On the other hand, in case of a dissociation equilibrium, the saturation profile is independent on protein concentration if the latter is $\leq K_D$ and the free ligand value is reported in the abscissa being approximate to the total ligand. The profile reported in figure allowed us to estimate $K_{D\_MANT\text{-}GTP} \ll 1$ μM.

MANT-GTP displacement

The displacement of MANT-GTP was carried out following the decrease in fluorescence of the MANT-GTP/DUAL complex (5 and 1 μM, respectively) in 20 mM Tris-Hcl pH 7.6, 150 mM NaCl and 2.5 mM $MnCl_2$ upon the addition of different amounts GTP, GTPαS, GTPγS.

The maximum of the emission spectrum was used as fluorescence signal for displacement plot, once the value was base-line corrected. For displacement experiments, data were fitted with the following displacement equation [57]:

$$f_x = f_{bott} + \frac{(f_0 - f_{bott})}{1 + 10^{(\log x - \log K_{app})}}$$

being x the concentration of each GTP species used from displacement experiments, f_x the fluorescence signal at each GTP addition, f_0 the fluorescence of the MANT-GTP/DUAL complex when no competitor is present, f_{bott} the fluorescence of 5 μM MANT-GTP in the presence of the maximal concentration of GTP species used for each displacement; data fit was corrected for the slope of the free MANT-GTP signal. K_{app} is the displacement constant, corresponding to the concentration of competitor required to obtain 50% of displacement. K_{app} depends on K_{D_GTP}, $K_{D\_MANTGTP}$ and [MANT-GTP] used in the assay according to the following equation:

$$K_{app} = K_{D\_GTP} * (1 + \frac{[\mathrm{MANT-GTP}]}{K_{D\_MANTGTP}})$$

K_{displ} reported in the figure legends represents the mean value of two independent experiments ± SD.

Isothermal titration calorimetry (ITC) assays

Isothermal titration calorimetry (ITC) experiments were carried out using an iTC200 microcalorimeter (MicroCal). Binding of c-di-GMP to EAL-2 and to DUAL (the latter with or without 50 μM GTP in the protein and in the ligand solutions) was assayed at 25 °C, by titrating 35 μM or 25 μM protein with 195 μM or 390 μM c-di-GMP, respectively. 1.2 μL aliquots of c-di-GMP solution (in the same buffer of protein solution) were injected into the protein solution with a time interval between injections of 200 s.

ITC data on EAL-2 were analysed by integrating the heat exchange for each addition and normalized for the amount of injected protein. As acknowledged by the literature, the first points of the titration, even though they are baseline-corrected, have not been considered in the fit, being biased by the high endothermic contribution due to c-di-GMP dilution into the cell [58,59].

The heat of binding (H), the stoichiometry (n), and the dissociation constant (K_D) were then calculated from plots of the heat evolved per mole of ligand injected versus the molar ratio of ligand to protein using the ORIGIN (OriginLab Corporation) software provided by the vendor (single binding site equation). Data are the mean of at least three experiments ± SD. Titration of DUAL shows a very complicated profile which could be fitted both with the two-binding sites equation or the sequential-binding (i.e., cooperativity) site equation provided by the vendor, yielding a comparable fit residual (but deeply different from a mechanistic point of view). The first process is a mixture of highly endothermic and exothermic events, which cover the events occurring at higher ligand concentration. At this stage we could speculate that the endothermic events (leading to the V-shaped curve) accounts not only for the dilution of c-di-GMP, which is highly endothermic as mentioned above, but also for dramatic rearrangement and desolvation events (as in the case of metal binding to the active site). This behaviour has been observed for other hybrid proteins to a lower extent and the authors did not discern the multitude of events [8,59]. Accordingly, we do not present a data fitting given that the molecular bases of such profile are unknown. Given the complexity of the events, we prefer to consider quantitatively only FRET data.

Dynamic light-scattering measurements

Dynamic light-scattering measurements on protein solutions were carried out with a Zetasizer Nano S (Malvern Instruments, Malvern, UK) equipped with a 4 mW He–Ne laser (633 nm). Measurements were performed at 25 °C at an angle of 173° from the incident beam with a protein concentration of 4 μM in PDE buffer in the presence of $MnCl_2$ 2.5 mM. Peak-intensity analyses were used to determine hydrodynamic radius number distribution (Pn) in the presence and in the absence of GTP at a final concentration of 50 μM. Both conditions have been tested twice, and each measurement is the result of the average of 24 consecutive measurements.

Determination of the aggregation state of DUAL by SEC

Hundred microlitre of a protein solution containing DUAL (40 μM) were injected into a TSKgel G3000PWxl HPLC column (Tosoh Bioscience, San Francisco, CA, USA) equilibrated with 150 mM NaCl, 20 mM Tris/HCl pH 7.0, 2.5 mM $MgCl_2$, 2.5 mM $MnCl_2$, ± 300 μM GTP (GE Healthcare) and mounted on a HPLC dual pump system Azura ASM2.1L (Knauer, Berlin, Germany). The column was calibrated by running in the same buffers the following standards (GE Healthcare): Ferritin (440 kDa), Tyroglobin (669 kDa), Aldolase (158 kDa), Conalbumin (75 kDa). The aggregation state is dimeric for all the constructs and has been verified by AUC (not shown). Protein sample with GTP was run after 10 min of incubation with this nucleotide.

Statistical analysis

Statistical differences were determined by one-way analysis of variance followed by Student's *t*-test with the Bonferroni correction. $P \leq 0.05$ was considered significant.

Acknowledgements

The authors would like to acknowledge Ministero della Università e Ricerca of Italy [RBFR10LHD1 to SR and GR] and Sapienza University of Rome [to FC, SR and AP] for financial support. A special thank to Daniela Verzili and Carlotta Zamparelli for AUC measurement, Francesco Malatesta and Luciana Mosca for useful discussions, Giovanna Boumis for technical support.

Author contributions

FM contributed kinetics and binding experiments; AP contributed the bioinformatics study and to write the manuscript; PB contributed bio-crystallography experiments; CDA and LC contributed the kinetic and binding characterization of DUAL; APaone, LL and GR contributed molecular biology experiments; LC, RP and MR contributed RP-HPLC optimization; AA contributed DLS experiments, GG supervised the crystallographic experiments, performed data processing and model-building and contributed to write the manuscript, FC supervised the group and wrote the manuscript with SR, SR supervised kinetics and binding experiments and wrote the manuscript.

References

1 Romling U, Galperin MY & Gomelsky M (2013) Cyclic di-GMP: the first 25 years of a universal bacterial second messenger. *Microbiol Mol Biol Rev* **77**, 1–52.
2 Krasteva PV & Sondermann H (2017) Versatile modes of cellular regulation via cyclic dinucleotides. *Nat Chem Biol* **13**, 350–359.
3 Seshasayee AS, Fraser GM & Luscombe NM (2010) Comparative genomics of cyclic-di-GMP signalling in bacteria: post-translational regulation and catalytic activity. *Nucleic Acids Res* **38**, 5970–5981.

4 Phippen CW, Mikolajek H, Schlaefli HG, Keevil CW, Webb JS & Tews I (2014) Formation and dimerization of the phosphodiesterase active site of the *Pseudomonas aeruginosa* MorA, a bi-functional c-di-GMP regulator. *FEBS Lett* **588**, 4631–4636.
5 Christen M, Christen B, Folcher M, Schauerte A & Jenal U (2005) Identification and characterization of a cyclic di-GMP-specific phosphodiesterase and its allosteric control by GTP. *J Biol Chem* **280**, 30829–30837.
6 An S, Wu J & Zhang LH (2010) Modulation of *Pseudomonas aeruginosa* biofilm dispersal by a cyclic-Di-GMP phosphodiesterase with a putative hypoxia-sensing domain. *Appl Environ Microbiol* **76**, 8160–8173.
7 Liu C, Liew CW, Wong YH, Tan ST, Poh WH, Manimekalai SMS, Rajan S, Xin L, Liang ZX, Gruber G *et al*. (2017) Insights into biofilm dispersal regulation from the crystal structure of the PAS-GGDEF-EAL region of RbdA from *Pseudomonas aeruginosa*. *J Bacteriol* **200**, e00515–e00517.
8 Navarro MV, De N, Bae N, Wang Q & Sondermann H (2009) Structural analysis of the GGDEF-EAL domain-containing c-di-GMP receptor FimX. *Structure* **17**, 1104–1116.
9 Navarro MV, Newell PD, Krasteva PV, Chatterjee D, Madden DR, O'Toole GA & Sondermann H (2011) Structural basis for c-di-GMP-mediated inside-out signaling controlling periplasmic proteolysis. *PLoS Biol* **9**, e1000588.
10 Paiardini A, Mantoni F, Giardina G, Paone A, Janson G, Leoni L, Rampioni G, Cutruzzolà F & Rinaldo S (2018) A novel bacterial L-arginine sensor controlling c-di-GMP levels in *Pseudomonas aeruginosa*. *Proteins*. https://doi.org/10.1002/prot.25587
11 Ha DG, Richman ME & O'Toole GA (2014) Deletion mutant library for investigation of functional outputs of cyclic diguanylate metabolism in *Pseudomonas aeruginosa* PA14. *Appl Environ Microbiol* **80**, 3384–3393.
12 Okegbe C, Fields BL, Cole SJ, Beierschmitt C, Morgan CJ, Price-Whelan A, Stewart RC, Lee VT & Dietrich LEP (2017) Electron-shuttling antibiotics structure bacterial communities by modulating cellular levels of c-di-GMP. *Proc Natl Acad Sci U S A* **114**, E5236–E5245.
13 Stelitano V, Giardina G, Paiardini A, Castiglione N, Cutruzzola F & Rinaldo S (2013) C-di-GMP hydrolysis by *Pseudomonas aeruginosa* HD-GYP phosphodiesterases: analysis of the reaction mechanism and novel roles for pGpG. *PLoS One* **8**, e74920.
14 Chen MW, Kotaka M, Vonrhein C, Bricogne G, Rao F, Chuah ML, Svergun D, Schneider G, Liang ZX & Lescar J (2012) Structural insights into the regulatory mechanism of the response regulator RocR from *Pseudomonas aeruginosa* in cyclic Di-GMP signaling. *J Bacteriol* **194**, 4837–4846.
15 Barends TR, Hartmann E, Griese JJ, Beitlich T, Kirienko NV, Ryjenkov DA, Reinstein J, Shoeman RL, Gomelsky M & Schlichting I (2009) Structure and mechanism of a bacterial light-regulated cyclic nucleotide phosphodiesterase. *Nature* **459**, 1015–1018.
16 Tchigvintsev A, Xu X, Singer A, Chang C, Brown G, Proudfoot M, Cui H, Flick R, Anderson WF, Joachimiak A *et al*. (2010) Structural insight into the mechanism of c-di-GMP hydrolysis by EAL domain phosphodiesterases. *J Mol Biol* **402**, 524–538.
17 Sundriyal A, Massa C, Samoray D, Zehender F, Sharpe T, Jenal U & Schirmer T (2014) Inherent regulation of EAL domain-catalyzed hydrolysis of second messenger cyclic di-GMP. *J Biol Chem* **289**, 6978–6990.
18 Bellini D, Horrell S, Hutchin A, Phippen CW, Strange RW, Cai Y, Wagner A, Webb JS, Tews I & Walsh MA (2017) Dimerisation induced formation of the active site and the identification of three metal sites in EAL-phosphodiesterases. *Sci Rep* **7**, 42166.
19 Rao F, Qi Y, Chong HS, Kotaka M, Li B, Li J, Lescar J, Tang K & Liang ZX (2009) The functional role of a conserved loop in EAL domain-based cyclic di-GMP-specific phosphodiesterase. *J Bacteriol* **191**, 4722–4731.
20 Tarnawski M, Barends TR & Schlichting I (2015) Structural analysis of an oxygen-regulated diguanylate cyclase. *Acta Crystallogr D* **71**, 2158–2177.
21 Wassmann P, Chan C, Paul R, Beck A, Heerklotz H, Jenal U & Schirmer T (2007) Structure of BeF3- -modified response regulator PleD: implications for diguanylate cyclase activation, catalysis, and feedback inhibition. *Structure* **15**, 915–927.
22 Deepthi A, Liew CW, Liang ZX, Swaminathan K & Lescar J (2014) Structure of a diguanylate cyclase from *Thermotoga maritima*: insights into activation, feedback inhibition and thermostability. *PLoS One* **9**, e110912.
23 Batista PR, Robert CH, Marechal JD, Hamida-Rebai MB, Pascutti PG, Bisch PM & Perahia D (2010) Consensus modes, a robust description of protein collective motions from multiple-minima normal mode analysis–application to the HIV-1 protease. *Phys Chem Chem Phys* **12**, 2850–2859.
24 Kass I, Hoke DE, Costa MG, Reboul CF, Porebski BT, Cowieson NP, Leh H, Pennacchietti E, McCoey J, Kleifeld O *et al*. (2014) Cofactor-dependent conformational heterogeneity of GAD65 and its role in autoimmunity and neurotransmitter homeostasis. *Proc Natl Acad Sci U S A* **111**, E2524–E2529.
25 Chatterjee D, Cooley RB, Boyd CD, Mehl RA, O'Toole GA & Sondermann H (2014) Mechanistic insight into the conserved allosteric regulation of periplasmic proteolysis by the signaling molecule cyclic-di-GMP. *eLife* **3**, e03650.

26 Christen B, Christen M, Paul R, Schmid F, Folcher M, Jenoe P, Meuwly M & Jenal U (2006) Allosteric control of cyclic di-GMP signaling. *J Biol Chem* **281**, 32015–32024.
27 Weinhouse H, Sapir S, Amikam D, Shilo Y, Volman G, Ohana P & Benziman M (1997) c-di-GMP-binding protein, a new factor regulating cellulose synthesis in *Acetobacter xylinum*. *FEBS Lett* **416**, 207–211.
28 Koestler BJ & Waters CM (2013) Exploring environmental control of cyclic di-GMP signaling in *Vibrio cholerae* by using the ex vivo lysate cyclic di-GMP assay (TELCA). *Appl Environ Microbiol* **79**, 5233–5241.
29 Massie JP, Reynolds EL, Koestler BJ, Cong J-P, Agostoni M & Waters CM (2012) Quantification of high-specificity cyclic diguanylate signaling. *Proc Natl Acad Sci U S A* **109**, 12746.
30 Simm R, Morr M, Kader A, Nimtz M & Romling U (2004) GGDEF and EAL domains inversely regulate cyclic di-GMP levels and transition from sessility to motility. *Mol Microbiol* **53**, 1123–1134.
31 Simm R, Morr M, Remminghorst U, Andersson M & Romling U (2009) Quantitative determination of cyclic diguanosine monophosphate concentrations in nucleotide extracts of bacteria by matrix-assisted laser desorption/ionization-time-of-flight mass spectrometry. *Anal Biochem* **386**, 53–58.
32 Ochi K, Kandala J & Freese E (1982) Evidence that *Bacillus subtilis* sporulation induced by the stringent response is caused by the decrease in GTP or GDP. *J Bacteriol* **151**, 1062–1065.
33 Lopez JM, Dromerick A & Freese E (1981) Response of guanosine 5′-triphosphate concentration to nutritional changes and its significance for *Bacillus subtilis* sporulation. *J Bacteriol* **146**, 605–613.
34 Chiaverotti TA, Parker G, Gallant J & Agabian N (1981) Conditions that trigger guanosine tetraphosphate accumulation in *Caulobacter crescentus*. *J Bacteriol* **145**, 1463–1465.
35 Bittner AN, Kriel A & Wang JD (2014) Lowering GTP level increases survival of amino acid starvation but slows growth rate for *Bacillus subtilis* cells lacking (p) ppGpp. *J Bacteriol* **196**, 2067–2076.
36 Key J, Hefti M, Purcell EB & Moffat K (2007) Structure of the redox sensor domain of *Azotobacter vinelandii* NifL at atomic resolution: signaling, dimerization, and mechanism. *Biochemistry* **46**, 3614–3623.
37 Dahlstrom KM, Collins AJ, Doing G, Taroni JN, Gauvin TJ, Greene CS, Hogan DA & O'Toole GA (2018) A multimodal strategy used by a large c-di-GMP network. *J Bacteriol* **200**, e00703–e00717.
38 Mueller U, Förster R, Hellmig M, Huschmann FU, Kastner A, Malecki P, Pühringer S, Röwer M, Sparta K, Steffien M *et al.* (2015) The macromolecular crystallography beamlines at BESSY II of the Helmholtz-Zentrum Berlin: current status and perspectives. *Eur Phys J Plus* **130**, 141.
39 Kabsch W (2010) XDS. *Acta Crystallogr D* **66**, 125–132.
40 CCP4 (Collaborative Computational Project, N (1994) The CCP4 suite: programs for protein crystallography. *Acta Crystallogr D* **50**, 760–763.
41 McCoy AJ, Grosse-Kunstleve RW, Adams PD, Winn MD, Storoni LC & Read RJ (2007) Phaser crystallographic software. *J Appl Crystallogr* **40**, 658–674.
42 Giardina G, Paiardini A, Fernicola S, Franceschini S, Rinaldo S, Stelitano V & Cutruzzola F (2013) Investigating the allosteric regulation of YfiN from *Pseudomonas aeruginosa*: clues from the structure of the catalytic domain. *PLoS One* **8**, e81324.
43 Emsley P & Cowtan K (2004) Coot: model-building tools for molecular graphics. *Acta Crystallogr D* **60**, 2126–2132.
44 Murshudov GN, Skubák P, Lebedev AA, Pannu NS, Steiner RA, Nicholls RA, Winn MD, Long F & Vagin AA (2011) REFMAC5 for the refinement of macromolecular crystal structures. *Acta Crystallogr D* **67**, 355–367.
45 Nicholls RA, Long F & Murshudov GN (2013) Recent advances in low resolution refinement tools in REFMAC5. In *Advancing Methods for Biomolecular Crystallography* (Read R, Urzhumtsev AG & Lunin VY, eds), pp. 231–258, Springer Netherlands, Dordrecht.
46 Rinaldo S, Giardina G, Mantoni F, Paiardini A, Paone A & Cutruzzola F (2017) Discovering selective diguanylate cyclase inhibitors: from PleD to discrimination of the active site of cyclic-di-GMP phosphodiesterases. *Methods Mol Biol* **1657**, 431–453.
47 Stelitano V, Brandt A, Fernicola S, Franceschini S, Giardina G, Pica A, Rinaldo S, Sica F & Cutruzzola F (2013) Probing the activity of diguanylate cyclases and c-di-GMP phosphodiesterases in real-time by CD spectroscopy. *Nucleic Acids Res* **41**, e79.
48 Kelley LA, Mezulis S, Yates CM, Wass MN & Sternberg MJE (2015) The Phyre2 web portal for protein modeling, prediction and analysis. *Nat Protoc* **10**, 845–858.
49 Janson G, Zhang C, Prado MG & Paiardini A (2017) PyMod 2.0: improvements in protein sequence-structure analysis and homology modeling within PyMOL. *Bioinformatics* **33**, 444–446.
50 Bramucci E, Paiardini A, Bossa F & Pascarella S (2012) PyMod: sequence similarity searches, multiple sequence-structure alignments, and homology modeling within PyMOL. *BMC Bioinformatics* **13** (Suppl 4), S2.

51 Edgar RC (2004) MUSCLE: a multiple sequence alignment method with reduced time and space complexity. *BMC Bioinformatics* **5**, 113.
52 Rost B & Sander C (1994) Combining evolutionary information and neural networks to predict protein secondary structure. *Proteins* **19**, 55–72.
53 Paiardini A, Bossa F & Pascarella S (2005) CAMPO, SCR_FIND and CHC_FIND: a suite of web tools for computational structural biology. *Nucleic Acids Res* **33**, W50–W55.
54 Sali A, Potterton L, Yuan F, van Vlijmen H & Karplus M (1995) Evaluation of comparative protein modeling by MODELLER. *Proteins* **23**, 318–326.
55 Eisenberg D, Luthy R & Bowie JU (1997) VERIFY3D: assessment of protein models with three-dimensional profiles. *Methods Enzymol* **277**, 396–404.
56 Atilgan AR, Durell SR, Jernigan RL, Demirel MC, Keskin O & Bahar I (2001) Anisotropy of fluctuation dynamics of proteins with an elastic network model. *Biophys J* **80**, 505–515.
57 Motulsky HJ & Christopoulos A (2003) Fitting Models to Biological Data Using Linear and Nonlinear Regression. A Practical Guide to Curve Fitting. GraphPad Software Inc., San Diego, CA.
58 Paul R, Abel S, Wassmann P, Beck A, Heerklotz H & Jenal U (2007) Activation of the diguanylate cyclase PleD by phosphorylation-mediated dimerization. *J Biol Chem* **282**, 29170–29177.
59 Matsuyama BY, Krasteva PV, Baraquet C, Harwood CS, Sondermann H & Navarro MVAS (2016) Mechanistic insights into c-di-GMP–dependent control of the biofilm regulator FleQ from *Pseudomonas aeruginosa*. *Proc Natl Acad Sci U S A* **113**, E209–E218.

Supporting information

Additional supporting information may be found online in the Supporting Information section at the end of the article.

Table S1. Optimization of PDE activity of DUAL in the presence of excess GTP.

Table S2. Comparison of the catalytic properties of the PDE activity of RmcA with other EAL-containing proteins characterized so far.

Movie S1. Anisotropic Network Model used during NM analysis.

Movie S2. Closing of the DUAL monomer-A during NM analysis.